IOP Publishing and International Atomic Energy Agency Nuclear Fusion
Nucl. Fusion **49** (2009) 104025 (15pp) doi:10.1088/0029-5515/49/10/104025

Theory and observations of magnetic islands

F.L. Waelbroeck

Institute for Fusion Studies, The University of Texas, Austin, TX 78712, USA

Received 5 January 2009, accepted for publication 15 June 2009
Published 10 September 2009
Online at stacks.iop.org/NF/49/104025

Abstract
Magnetic islands are a ubiquitous feature of magnetically confined plasmas. They arise as the result of plasma instabilities as well as externally imposed symmetry-breaking perturbations. In the core, effective suppression techniques have been developed. Even thin islands, however, are observed to have nonlocal effects on the profiles of rotation and current. This has stimulated interest in using magnetic islands to control plasma transport, particularly in the edge. They are also of interest as a tool to improve our understanding of microscopic plasma dynamics.

PACS numbers: 52.35.Bj, 52.55.−s

(Some figures in this article are in colour only in the electronic version)

1. Introduction

A goal shared by most magnetic confinement concepts is to realize a configuration consisting of simply nested magnetic surfaces enveloping a closed field line, the magnetic axis [1, 2]. In practice, small departures from this ideal configuration cause the flux surfaces to break into chains of magnetic islands, where each island is a tube of flux with its own private magnetic axis [3–5]. The primary significance of the islands is that heat can flow rapidly across them by following the field lines [6–8]. As a result, magnetic islands represent a loss of confinement volume [9–13]. In the edge of stellarators, however, they serve a useful function by diverting the field so as to separate the hot plasma in the confinement region from the material surfaces [14–17].

The effect of magnetic islands depends strongly on their proximity to each other. The overlap of neighbouring chains of islands results in the destruction of the underlying flux surfaces. In the region of overlap, the magnetic field lines wander chaotically, giving rise to anomalous transport of electron momentum (hyperresistivity) as well as heat [18, 19]. Due to the dependence of the plasma conductivity on electron temperature, magnetic chaos affects the current profile through enhanced thermal diffusion as well as through hyperresistivity.

The consequences of magnetic chaos depend on the nature of the discharge as well as on the wavelength of the magnetic islands. Disruptions caused by the overlap of long-wavelength islands in the confinement region of tokamaks are the most dramatic consequence. The flattening of the temperature during sawtooth crashes is probably also caused by magnetic chaos [20–22]. In reversed field pinches (RFPs), by contrast, the interaction of islands of multiple scales contributes to the sustainment of the field reversal [23–25]. Reducing the island overlap, however, gives access to regimes with qualitatively improved confinement [26–28]. In spherical tokamaks, observations and modelling show that thin, short wavelength islands contribute to the turbulent transport of electron heat [29]. Lastly, in the edge of tokamaks, closely spaced externally driven chains of islands with moderate wavelengths are observed to cause anomalous particle transport under conditions of low-collisionality [30–32]. The simultaneous steepening of the electron temperature pedestal, however, raises questions as to the presence of magnetic chaos.

In tokamaks, the islands resulting from the growth of the neoclassical tearing mode (NTM) have attracted a great deal of attention due to the limitation they impose on plasma pressure. This led to the development of RF current-drive techniques for reducing the size of magnetic islands. [33–39]. As a result, islands are no longer perceived as a direct threat to tokamak confinement, except near the stability boundaries of ideal modes [40–43]. Evidence has accumulated, however, showing that even when they occupy only a small fraction of the confinement volume, magnetic islands have significant nonlocal effects, not only on the temperature profiles but also on the profiles of the current [44–46] and the rotation velocity [47–51]. This has fostered interest in using them as agents to control transport and stability properties. In addition, islands constitute a useful diagnostic tool for obtaining information on the current and rotation profiles [52]. Lastly, they provide a unique window into plasma dynamics at scales that are difficult to observe directly.

In this paper, I present an overview of the experimental and theoretical results concerning magnetic islands.

2. Magnetic islands as equilibrium structures

I restrict attention to islands that are thin but sufficiently large to affect the background profiles of the reference equilibrium: in present-day experiments this corresponds to perturbation amplitudes in the range $10^{-4} \lesssim \delta B/B \lesssim 10^{-3}$ [53–55]. The most direct approach to predicting the evolution of such as islands is by using a general-purpose initial-value magnetohydrodynamic (MHD) code [25, 40, 41, 56–60] or codes using other fluid models such as the drift model [61–68]. Hall-MHD [69] and neoclassical MHD [37, 70–74]. Due to the high conductivity of fusion plasmas, however, islands generally evolve very slowly compared with the Alfvén time. Away from marginal stability, saturation requires a fraction W/a of the skin time, where W is the island width and a is the minor radius. Even after artificially increasing the resistivity, long simulation times are required to describe saturation as well as to address the question of the role of changes in the profiles. This, together with the spatial resolution requirements, has severely restricted the scope of the problems that can be treated by direct numerical simulations. A more adapted approach is to use the time and space-scale separation to advantage by investigating islands from the point of view of the equilibrium and transport of three-dimensional (3D) helical plasmas. I elaborate on this approach below.

The analysis of 3D magnetostatic equilibria reveals a fundamental reason for the occurrence of magnetic islands. Specifically, it shows that in the absence of symmetry, an equilibrium with *simply nested* flux surfaces (i.e. free of magnetic islands) exhibits a current singularity on any flux surface where the magnetic field lines close on themselves and where the pressure gradient does not vanish. These current singularities are clearly unphysical: in the presence of plasma resistivity, they are resolved by magnetic reconnection and the breakup of the resonant magnetic surfaces into island chains. The size of the resulting island chains, however, is a sensitive function of plasma rotation and of the history of the discharge. I will summarize recent progress in understanding the interrelationship between magnetic islands and plasma rotation in sections 3 and 4.

To show the occurrence of current singularities in 3D equilibria, consider the hydrostatic equilibrium condition $\boldsymbol{J} \times \boldsymbol{B} = \nabla p$, where $\boldsymbol{B}$ is the magnetic field, $\boldsymbol{J} = \nabla \times \boldsymbol{B}/\mu_0$ is the current and p is a scalar pressure. Separating the components of the current in the directions parallel and perpendicular to the magnetic field, we note that force balance determines the perpendicular component of the current, $\boldsymbol{J}_\perp$, in terms of the pressure gradient [75]:

$$\boldsymbol{J}_\perp = B^{-1}\,\hat{\boldsymbol{b}} \times \nabla p,$$

where $B = |\boldsymbol{B}|$ is the amplitude of the magnetic field. Substituting the perpendicular current into the charge conservation law, $\nabla \cdot \boldsymbol{J} = 0$, results in a magnetic differential equation for the parallel component of the current, $J_\parallel$:

$$\boldsymbol{B} \cdot \nabla (J_\parallel/B) = -\nabla \cdot \boldsymbol{J}_\perp.$$

It is convenient to use field-line coordinates defined by $\boldsymbol{B} = \nabla\chi \times \nabla(\zeta - q\theta)$, where θ and ζ are poloidal and toroidal coordinates, respectively, χ is a poloidal flux function that labels the simply nested, non-axisymmetric flux surfaces and $q = q(\chi)$ is the safety factor that is a function of χ only [75]. Note that $\boldsymbol{B} \cdot \nabla\chi = 0$. Furthermore, the equilibrium equation implies that $p = p(\chi)$. Fourier expansion using these coordinates yields the solution

$$\left[\frac{J_\parallel}{B}\right]_{m,n} = \frac{\mu_0 p'(\chi)}{\langle B^2\rangle} \sum_{m,n} \frac{\mathcal{G}_{m,n}(\chi)}{q(\chi) - m/n} + \hat{J}_{m,n}\,\delta(q(\chi) - m/n), \tag{1}$$

where the m, n subscripts denote the Fourier indices of the corresponding variables, the $\mathcal{G}_{m,n}$ are geometrical factors, the $\hat{J}_{m,n}$ are integration constants, $p'(\chi) = \mathrm{d}p/\mathrm{d}\chi$ and $\langle\cdot\rangle$ represents the average over a flux surface,

$$\langle B^2\rangle = \oint\oint \frac{\mathrm{d}\theta\,\mathrm{d}\zeta}{|\boldsymbol{B}\cdot\nabla\theta|}\,B^2. \tag{2}$$

The $\mathcal{G}_{m,n}$ are regular functions of χ. With the exception of perfectly symmetric systems, they do not vanish at $q(\chi) = m/n$ so that the parallel component of the current is singular on every flux surface with a rational safety factor q. In general, the equilibrium is dominated by a small number of surfaces corresponding to $n = 1$, 2 and (more rarely) $n = 3$. The corresponding $q = m/n$ surfaces are called the resonant surfaces.

As noted previously, in a resistive plasma the current singularities bring about magnetic reconnection and the breakup of the resonant magnetic surfaces into island chains. The primary object of the island theory is to calculate the effect of the island on confinement. The key parameters that determine this effect are the width and either the rotation frequency (in the case of intrinisic tearing modes) or the phase (in the case of externally applied perturbations) of the resulting islands. It is important to keep in mind, however, that the width of an island is not merely a local property but that it measures the amplitude of the 'tearing' component of the wavefunction *in the entire device* [76]. In fact, rotating islands in the core of tokamaks were first observed through oscillations of the magnetic field at the edge, the so-called Mirnov oscillations [3]. Even in the absence of rotation, the growth of magnetic islands driven by external resonant magnetic perturbations (RMPs), the so-called 'locked modes', gives rise to clear signals on external magnetic detectors, providing further evidence of the global nature of the tearing wavefunction associated with magnetic islands [53–55, 77–80].

2.1. Method of matched asymptotic expansions

Due to the singular nature of the perturbation, it is helpful to divide the plasma into two sets of overlapping regions. The first set comprises the *resonant layers* consisting of thin annuli containing the resonant surfaces of interest. The second set regroups the *exterior regions* and consists of the bulk of the plasma volume from which thin annuli enclosing the resonant surfaces have been excised. In principle, the asymptotic matching between the solutions in the resonant layers and the solutions in the exterior regions provides a complete determination of the spatial dependence of the perturbation.

Pletzer *et al* [81] have used the method of matched asymptotic expansions to calculate the growth rate of a tearing mode in a torus. They demonstrated good agreement between

the growth rates obtained with the asymptotic method and those obtained with MARS, a full-torus, finite-element code that solves the same problem without asymptotic matching. More recently, Escande and Ottaviani [82] and Militello *et al* [83] have demonstrated good agreement between the asymptotic results for the saturation amplitudes of magnetic islands in a slab and those obtained with a nonlinear initial-value code. Most investigators, however, confine themselves to using analytic or even heuristic models for either the layer or the exterior solutions.

Within the resonant layers, the ideal MHD model is inadequate and effects such as diamagnetic drifts, finite Larmor radius and Landau damping need to be taken into account. This is a formidable problem that is the subject of ongoing research. The analysis is facilitated, however, by the fact that the variation of the background parameters is negligible within the layers, since $q - m/n \ll 1$.

Outside the layers, by contrast, it is necessary to use the complete, ideal, hydrostatic MHD model to describe the distortion of the equilibrium [84–86]. In order to address the effect of the island on the equilibrium profiles, however, the MHD calculation must be supplemented by a transport calculation [30, 47, 87–90]. The helical equilibrium outside the layer is sensitive to the imposed geometry as well as to the current and pressure profiles, so that its calculation generally requires a numerical approach. The following section describes the approaches to the description of the plasma in the exterior region.

2.2. *Exterior solution in axisymmetric systems*

Even when the asymmetry of the coils and confinement vessel is negligible, the plasma may nevertheless adopt an asymmetric configuration as the result of an equilibrium bifurcation. In the exterior region, it is then generally appropriate to linearize the solution about an unperturbed equilibrium described by a symmetric magnetic field $\boldsymbol{B}_0$. Matching the exterior solution to the solution in the singular layer(s) requires knowledge of the parallel component of the vector potential, denoted by $\tilde{\psi} = \boldsymbol{B}_0 \cdot \tilde{\boldsymbol{A}}/B_0$. The quantity $\tilde{\psi}$ represents a magnetic flux, and is proportional to the displacement of the flux surfaces.

The standard code for calculating a spontaneous symmetry-breaking perturbation for low values of the toroidal mode-number n is the venerable PEST-III [91], which calculates both the tearing-parity and twisting-parity (interchange) wavefunctions in tokamaks with an axisymmetric boundary condition. A simplified picture of PEST-III's function is that for a given n and an equilibrium with M singular surfaces, it calculates a matrix relating the M amplitudes $\hat{J}_{m,n}$ of the delta functions in equation (1) to the asymptotic amplitudes $\tilde{\psi}_{m,n}$ of the flux perturbation at the M singular surfaces. We will refer to this matrix as the matching matrix. Note that due to processes taking place in the layer, the actual value of $\tilde{\psi}_{m,n}$ at the resonant surface may differ from its asymptotic value extrapolated from the exterior region. The amplitude of the singular current, on the other hand, is proportional to the jump in the magnetic field across the layer, $\hat{J}_{m,n} = \nabla\chi \cdot [\nabla\tilde{\psi}]/|\nabla\chi|$, where $[\cdot]$ describes the jump across the layer.

At the resonant surface, the parallel component of the electrostatic field vanishes since $k_\parallel = 0$, so that $(E_\parallel)_{m,n} = -\mathrm{i}\omega\tilde{\psi}_{m,n}$, where ω is the mode frequency and $E_\parallel$ is the parallel component of the electric field. Fixing n and denoting the elements of the matching matrix by $-\mathrm{i}\omega Y_{mm'}$, there follows

$$\hat{J}_m = -\mathrm{i}\omega \sum_{m'} Y_{mm'}\tilde{\psi}_{m'} = \sum_{m'} Y_{mm'} E_{\parallel,m'}, \tag{3}$$

so that the $Y_{mm'}$ may be interpreted as an admittance matrix for launching Alfvén waves from the resonant surfaces.

In the special case where the plasma contains only a single resonant surface for the given toroidal mode-number n, equation (3) reduces to

$$[\psi'_m] = \Delta'_m \tilde{\psi}_m, \tag{4}$$

where $[\psi'_m]$ describes the jump in the derivative of the flux perturbation across the singular layer and $\Delta'_m = -\mathrm{i}\omega\mu_0 Y_{mm}$ is the usual tearing stability parameter introduced by Furth *et al* [84] (see also [75] for a textbook introduction to tearing modes) Thus, in the single-resonance case, the Y matrix reduces to a scalar proportional to the Δ' parameter. An important property of this parameter is that it grows without bounds as the plasma approaches ideal marginal stability (as a result of rising β, for example) [41, 92]. This is a manifestation of the approach of an *ideal* equilibrium bifurcation. Chu *et al* have successfully applied the PEST-III code to analyse the onset of tearing modes, corresponding to a *resistive* equilibrium bifurcation, in current ramp experiments on the DIII-D tokamak [93].

Another special case of interest is that of a cylindrical plasma, where the coupling between the various poloidal harmonics vanishes. In this case, the matching matrix takes a diagonal form, with the diagonal elements given by $Y_{mm} = \mathrm{i}\Delta'_m/\omega\mu_0$.

An alternative to the direct calculation of the matching matrix is to extract it from initial-value simulations using a resistive MHD code [94]. The idea of this approach is that the matching matrix can subsequently be used with a more realistic model for the dynamics inside the tearing layer. For high-n modes, this method and PEST-III both have difficulty converging, but the ballooning transformation makes it possible to calculate the matching matrix by integrating a one-dimensional equation along the field line [92].

An ongoing effort to replace PEST-III by a code that allows for inhomogeneous boundary conditions, models realistically the geometry of the coils and uses more advanced numerical techniques is making steady progress. The current embodiment of this effort, the Ideal Perturbed Equilibrium Code (IPEC), calculates the ideal component of the wavefunctions driven by RMPs, such as those caused by field errors and control coils [95]. It thus plays a role complementary to PEST-III, which calculates the wavefunctions for homogeneous boundary conditions. The complete specification of the perturbed equilibrium requires both codes in addition to a model for the response of the plasma in the resonant layers. Among other present-day applications, IPEC serves to guide the design of error-field correction coils [96].

For equilibria with weak shaping and large aspect ratio, the code T7 provides a nimble but imprecise evaluation of the matching matrix [97]. In addition to the matching matrix,

this code also calculates the coupling coefficients between the resonant surfaces and external perturbations, thereby allowing the investigation of braking and mode penetration [98]. It thus combines the functionality of PEST-III and IPEC, but only for a very limited class of equilibria.

2.3. Exterior solution in stellarators

Unlike for tokamaks, in stellarators the reference state itself contains current singularities, but their amplitude is minimized by design. Equilibrium codes for stellarators separate into those that assume simply nested magnetic surfaces, such as VMEC [99] and those that allow for magnetic islands, such as HINT and PIES [100, 101]. Simulations with the HINT code have shown that the geometry of the exterior region can lead to island healing [102]. Such a healing mechanism is distinct from that predicted by the layer theory, the latter depending only on the local value of the magnetic well at the resonant surface [103–105]. Generally speaking, global island codes serve to identify the qualitative effects of the overall geometry. Their partial or complete omission of effects that are important in the layer, however, such as convective transport near the separatrices, polarization currents and the role of viscosity on the phase of the island, prevents them from predicting the observed island widths and can lead to differences in their results [100]. Boozer and Nürenberg have developed an alternative approach that provides opportunities for including these effects by combining the VMEC nested-surface equilibrium code with the CAS3D linear stability code in order to determine the amplitudes $\hat{J}_{m,n}$ of the singular currents [85, 86]. One may subsequently determine the characteristics of the island by applying an appropriate model describing the plasma in the singular layer.

2.4. Solution in the singular layer

For thin islands, the rapid variation of the current across the island suggests the use of the flute ordering [2, 106],

$$\nabla_\parallel \sim L^{-1} \ll \nabla_\perp \sim W^{-1},$$

where L represents an equilibrium scale-length. The flute ordering leads to a reduced description of the nonlinear dynamics of short wavelength Alfvénic modes that is locally accurate, in contrast with the reduced-MHD (RMHD) model that provides a global but approximate description. In particular, the flute-RMHD theory correctly represents the effects of average normal curvature in the Mercier criterion, and it applies in geometries where RMHD fails, such as RFPs and spherical tokamaks.

Justifying the application of flute reduction to long-wavelength islands requires some care due to the circumstance that some quantities, such as $\tilde{\psi}$ for example, vary slowly across the singular layer. Flute reduction thus requires distinguishing three scale-lengths [106],

$$\nabla_\parallel \tilde{f} \ll L^{-1} \tilde{f} \ll |\nabla \tilde{f}|, \tag{5}$$

where $\tilde{f}$ is the resonant part of the perturbation experienced by a field f. It follows from equation (5) and $\nabla \cdot \boldsymbol{B} = 0$ that the magnetic field may be expressed as

$$\boldsymbol{B} = B_0 R_0 \nabla\zeta + \nabla\zeta \times \nabla\chi. \tag{6}$$

Here R_0 is the major radius, B_0 is the amplitude of the background magnetic field, ζ is the toroidal angle and $\chi = \chi_0 + \psi$ is the perturbed flux, where χ_0 is the poloidal flux corresponding to a reference state consisting of closed field lines of helicity $q_s = m/n$, and ψ is the helical flux which describes the sheared part of the background magnetic field as well as the magnetic perturbation. In order for the flute ordering, equation (5), to apply nonlinearly as well as linearly, it is necessary that $\tilde{\boldsymbol{B}} \cdot \nabla \tilde{f} \sim \boldsymbol{B}_0 \cdot \nabla \tilde{f}$ both be small, or that

$$\tilde{\boldsymbol{B}}/B_0 \sim k_\parallel W \ll 1. \tag{7}$$

The thin-island version of the flute ordering is consistent with that used to derive the gyrokinetic equation, so that gyrokinetic models may be used in the resonant layer region [107–109]. Note that the flute ordering implies that the non-resonant sidebands are smaller than the resonant harmonics by a factor of $k_\parallel L$. For long-wavelength modes ($k_\theta r_s \sim 1$, where r_s is the radius of the singular surface), the gradients of the perturbations are approximately perpendicular to the flux surfaces. In principle, this allows for a 1.5D treatment of 2D [6, 110] as well as 3D problems [111–113]. Even when they are focused on resonant layer processes, however, numerical simulations are often carried out in 2D slab geometry [61, 114–118].

The theory of the resonant layer divides into the linear and nonlinear regimes depending on the relative width of the island and the tearing layer. The rest of this section briefly describes each regime and its relevance to experiments. These descriptions are intended to serve as an introduction to the more detailed description of the principal experimental manifestations of these two regimes, which are given in sections 3 and 4, respectively.

2.4.1. Linear regime. In the linear regime, it is important to distinguish the case of intrinsic tearing modes from that of modes driven by RMPs. For intrinsic tearing modes, the dispersion relation determines the frequency of the mode, whereas for driven tearing modes, the applied perturbation determines the frequency.

For intrinsic tearing modes, the balance between the pressure gradient and the electric field on the resonant surface implies that the mode frequency is such as to match the perpendicular velocity of the electron fluid. It follows that for the collision frequencies characterizing present and future fusion experiments, the layer width for intrinsic tearing modes exhibits different scales characterizing the response of the electrons and the ions. The narrowest width, set by the electron dynamics, is smaller than the ion Larmor radius, so that experimentally observable intrinsic tearing modes are always in the nonlinear regime.

For driven tearing modes, by contrast, the electrons and ions are both streaming rapidly past the perturbations. This has the effect of greatly broadening the layer width, so that linear theory has a much wider domain of applicability. In fact, the description of these modes requires the consideration of *quasilinear* effects, since the forces they exert on the plasma change the background profiles. For example, the $\tilde{\boldsymbol{J}} \times \tilde{\boldsymbol{B}}$ force exerts a torque that changes the profile of the plasma rotation. Note that inertial effects are locally important for driven modes,

but that force-balance nevertheless, applies globally across the layer.

Section 3 describes the shielding of RMPs by rotating plasmas [119], the braking of plasma rotation and the failure of shielding manifested by mode penetration [76]. The theory accounting for these observations has enjoyed remarkable success despite being limited until recently to a low-beta MHD model.

2.4.2. Nonlinear regime. When the island width exceeds the linear tearing layer width for the electrons or ions, the dissipative terms become sub-dominant for the corresponding species of particles. This may occur either as a result of the growth of an intrinsic tearing mode or as a result of the onset of a locked mode, as described in section 3.

The case when the island width exceeds the layer widths of both species describes relaxed islands such as NTMs [120–125], snakes [126, 127] and the islands created in the edge of stellarators [128–130]. In the relaxed regime, force balance is satisfied locally. That is, the island represents a 3D equilibrium (although this equilibrium is generally not hydrostatic). The island modifies the equilibrium profiles, giving rise to flattening and sometimes local peaking of the profiles around the O-point. Section 4 will describe the relaxed, fully nonlinear regime.

3. Response of the plasma to RMPs

RMPs have a Fourier component that has the same winding ratio as the magnetic field on one or more magnetic surfaces lying within the plasma. They are a common occurrence in fusion experiments, resulting from internal MHD events such as sawteeth, fishbones and edge localized modes (ELMs), as well as from errors in the alignment of magnetic field coils and deliberately imposed plasma distortions. Due to their resonant nature, they have surprisingly large, nonlocal effects on plasma confinement. There is consequently a great deal of interest in using RMPs produced by external coils to control the plasma. This section surveys some of the relevant results. A detailed presentation of the MHD theory of RMPs can be found in a landmark paper by Fitzpatrick [76].

When the plasma is rotating, RMPs induce shielding currents that severely inhibit magnetic reconnection and limit the islands to very small widths [76, 119, 131, 132]. In addition to their role in shielding, the currents also allow the plasma to flow through the islands by Ohmic diffusion, thereby allowing the rotation of the plasma to continue despite the presence of an island. The resonant layer, nevertheless, constitutes an impediment to the flow that manifests itself as a braking force on the plasma rotation. An alternative interpretation for the braking is that kinetic energy must flow into the layer in order to replace the Ohmic power dissipated by the screening currents [131].

In the plasma frame, it is natural to interpret the perturbation as an Alfvén wave. At high frequency the wave exhibits near each rational surface a pair of resonances corresponding to $k_\parallel = \pm\omega/V_A$, where V_A is the Alfvén velocity. If the rotation frequency is reduced, the resonances overlap and then merge but the reconnected flux remains small until the frequency becomes comparable to the growth rate

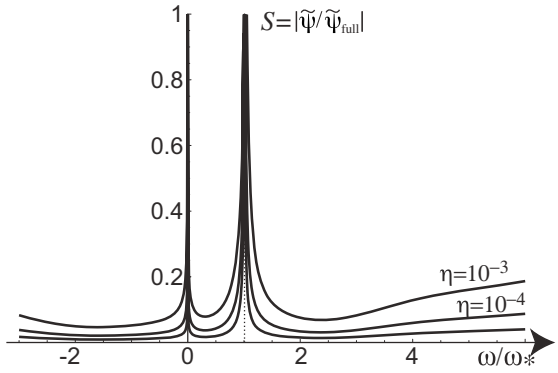

Figure 1. Variation of the screening factor $\mathcal{S} = \tilde{\psi}/\tilde{\psi}_{\rm full}$ with the plasma frequency for a cold-ion drift model. The parameters of the calculations are such that the ion-sound Larmor radius ρ_s is equal to the tearing layer thickness. The three curves correspond to values of the resistivity $\eta = 10^{-3}$, 10^{-4} and 10^{-5} (lowest curve).

of the tearing mode. At the resonance, momentum carried by the Alfvén wave may be transferred to the plasma through the action of the electromagnetic force $\boldsymbol{F}_{\rm EM} = \langle \tilde{\boldsymbol{J}} \times \tilde{\boldsymbol{B}} \rangle$, in a quasilinear process. Section 3.1 begins by describing the linear response.

3.1. Screening

The matching procedure described in section 2.1 yields the equation governing the plasma response,

$$\Delta' \tilde{\psi} + \tilde{B}^{\rm ext}_\theta(r_s) = \Delta(\omega)\tilde{\psi}, \tag{8}$$

where the mode numbers are omitted for clarity. Here ω is the perturbation frequency in the plasma frame (the frame where the electric field vanishes). If the perturbation is fixed in the lab frame, $\omega = -\omega_E$ where ω_E is the $\boldsymbol{E} \times \boldsymbol{B}$ frequency. Each side of equation (8) describes the jump in the total $\tilde{B}_\theta$ across the layer, the left-hand side representing the result of the exterior calculation and the right-hand side representing the result of the interior calculation. The term proportional to Δ' is the contribution of the tearing wavefunction. The $B^{\rm ext}_\theta(r_s)$ term represents the contribution that is driven directly by the external perturbation (i.e. the RMP). The calculation of this term is one of the functions of the IPEC.

In the absence of rotation, the island grows to a saturated state corresponding to continuous $\tilde{B}_\theta$. The reconnected flux in the saturated state is $\tilde{\psi}_{\rm full} = -\tilde{B}^{\rm ext}_\theta(r_s)/\Delta'$. The matching condition, equation (8), may thus be expressed as $\tilde{\psi} = \mathcal{S}(\omega)\tilde{\psi}_{\rm full}$, where $\mathcal{S}(\omega)$ is a screening factor given by

$$\mathcal{S}(\omega) = [1 - \Delta(\omega)/\Delta']^{-1}.$$

Note that $\mathcal{S}$ is generally complex. For rotation frequencies larger than the growth rate of the tearing mode, $\Delta(\omega) \gg \Delta'$ so that $|\mathcal{S}| \ll 1$. Figure 1 shows a sketch of the screening factor for a cold-ion, 'two-fluid' model of the plasma. The dominant features of this graph are the sharp resonances corresponding to rotation such that the ions ($\omega = 0$) and electrons ($\omega = \omega_{*e}$) are at rest, thereby enabling reconnection to proceed [119, 133, 134]. Note that for the sake of readability, figure 1 shows screening curves corresponding to values of η much larger than encountered in fusion experiments.

The rotation frequency is itself determined by the balance between the quasilinear electromagnetic braking force exerted by the perturbation, $\boldsymbol{F}_{\rm EM} = \langle \tilde{\boldsymbol{J}} \times \tilde{\boldsymbol{B}} \rangle$, and the viscous force exerted by the plasma. Section 3.2 next shows that the evolution of the frequency exhibits discontinuous transitions for critical values of either the perturbation amplitude or the momentum source in the plasma.

3.2. Resonant braking

Due to the rotation of the plasma, a phase-lag appears between the island and the current in the resonant layer. This phase-lag causes the perturbation to exert an electromagnetic $(\boldsymbol{J} \times \boldsymbol{B})$ force on the plasma. The net electromagnetic force acting on the plasma in the resonant layer is perpendicular to the unperturbed $\boldsymbol{B}(r_{\rm s})$ and tangent to the flux surface. The corresponding stress (force per unit area) is

$$F_{\rm EM} = -(k_\theta \Delta'/\mu_0)\, |\tilde{\psi}_{\rm full}|^2\, \Im[\mathcal{S}(\omega(r_{\rm s}))],$$

where μ_0 is the vacuum permeability, k_θ is the poloidal wavevector and $\Im$ represents the imaginary part. The electromagnetic force is opposed by a viscous force $F_{\rm v}$ representing the diffusive flow of momentum into the layer. The perpendicular component of the corresponding stress is [76]

$$F_{\rm v} = \frac{\mu}{k_\theta} \left(\frac{B}{B_\theta} \right)^2 [\delta\omega'(r_{\rm s}+0) - \delta\omega'(r_{\rm s}-0)].$$

Here μ is the viscosity coefficient, $\delta\omega(r)$ represents the change in the profile of the rotation frequency caused by the RMP and the primes denote radial derivation. The factor $(B/B_\theta)^2$ accounts for the neoclassical damping of the poloidal rotation. Integrating the momentum equation across the layer in steady-state conditions yields the force balance condition, $F_{\rm EM} = F_{\rm v}$.

The solution of the force balance equation may be pictured geometrically by graphing the forces as a function of the plasma rotation frequency at the resonant surface. It is convenient to normalize the forces to $|\tilde{\psi}_{\rm full}|^2$. The graph of the normalized electromagnetic force is then independent of the amplitude of the RMP and depends only on the properties of the equilibrium. Figure 2 shows the normalized electromagnetic force predicted by the MHD model. For simplicity we may make the approximation that the viscosity is independent of the rotation velocity of the plasma. With this approximation, the viscous force is proportional to the change in the rotation velocity at the resonant surface and is thus represented by a straight line (labeled $F_{\rm v}$) in figure 2. The intersection of this line with the abscissa specifies ω_0, the rotation frequency at the resonant surface in the absence of RMP. Its intersection with the electromagnetic force curve (point A) specifies $\omega_{\rm A}$, the rotation frequency at the resonant surface in the presence of the RMP. The reduction of the rotation frequency from ω_0 to $\omega_{\rm A}$ is a manifestation of *resonant braking* by the RMP. Section 3.3 considers the effect of varying the momentum source acting on the plasma.

3.3. Mode penetration

Changing the differential frequency between the plasma and the RMP (either by rotating the RMP or by varying the torque

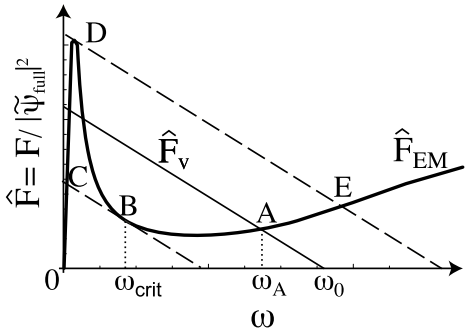

Figure 2. Sketch of the normalized forces showing the graphical solution for the island propagation velocity and the critical thresholds for mode penetration and island unlocking when the momentum input is changed. The parallel straight lines represent the viscous force and the curved line represents the normalized electromagnetic force.

exerted by the neutral beam injection (NBI) system) affects the graph by translating the viscous force line parallel to itself. A key feature of the curve describing the electromagnetic force is that it displays a minimum as a function of the rotation velocity. As a result, the balance between the viscous and electromagnetic forces exhibits a tangent bifurcation as the amplitude of the momentum input decreases (moving from point A to B in figure 2). As the system goes through the bifurcation, its state changes abruptly from point B to C, corresponding to negligible plasma rotation. After the bifurcation, the island grows rapidly up to its full width, as shown in figure 3. The full width of the relaxed island is generally somewhat larger than the vacuum width due to the phenomenon of resonant field amplification [42, 55, 135].

The fully reconnected island is called a *locked mode* and the bifurcation described above is known as *mode penetration*, or alternatively as a *locked-mode onset* [76, 79]. We avoid the practice of referring to mode penetration as 'mode-locking', however, preferring to reserve the latter term for the process whereby a rotating island produced by an intrinsic tearing mode ceases to rotate due to its interaction with external perturbations or with a resistive wall. Figures 2 and 3 show that mode penetration exhibits hysteresis. That is, if one increases the momentum input after the bifurcation, the reverse bifurcation does not occur until point D where the momentum input is considerably higher than that corresponding to the mode penetration. During the reverse bifurcation, the island is torn away from the RMP by the plasma flow and starts to rotate. Once its phase varies with respect to that of the RMP, the average drive provided by the RMP becomes stabilizing and the island heals (the average drive is due to the modulation of the island velocity as it rotates past the RMP). Note that in the fully reconnected state described by the segment between C and D, nonlinear effects will generally modify the electromagnetic force curve. The qualitative behaviour, however, is similar to that predicted by the quasilinear theory.

Instead of changing the momentum input or rotating the RMP, it is generally easier in experiments to change the strength of the applied perturbation. The variation of the viscous force curves with perturbation amplitude is rather difficult to evaluate, however, due to neoclassical toroidal viscosity (NTV), a drag force caused by the magnetic

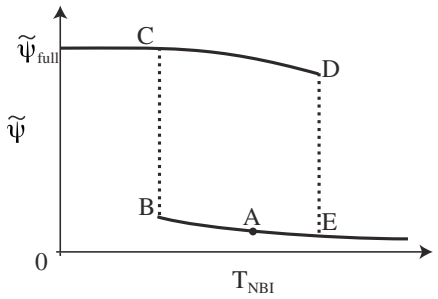

Figure 3. Sketch of the reconnected flux as a function of the momentum input (represented here by $T_{\rm NBI}$, the torque exerted by the NBI system). The lower curve represents the reconnected flux in a screened island and the upper curve represents the reconnected flux after mode penetration. The transitions clearly display hysteresis. The labelling of the characteristic points on the curves refers to the corresponding points in the force diagram (figure 2).

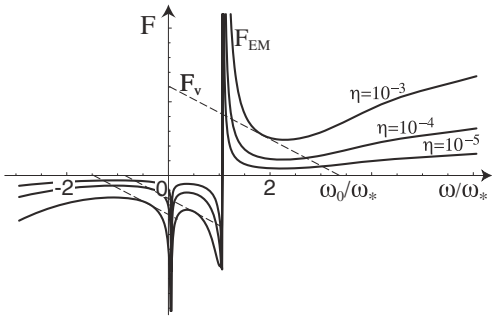

Figure 4. Sketch of the electromagnetic and viscous forces for the drift model. Mode penetration fixes the rotation velocity at $\omega \simeq \omega_{*e}$. The dashed lines show three viscous force curves corresponding to tangent bifurcations. Inspection of figure 1 shows that screening is maintained for the left-most bifurcation.

perturbation that acts on the entire plasma rather than only on the resonant layer. As a result of this drag force, both the slope and the intercept of the viscous force curves vary with $\tilde{\psi}$. Analysis of braking observations on JET and NSTX indicates that NTV dominates the overall braking process [47, 90], but its contribution to the local force balance at the resonant surface is negligible.

3.4. Effects of drifts and low collisionality

Due to the high temperature of fusion plasmas, deviations from MHD theory are important especially in internal transport barriers and in the edge pedestal where diamagnetic drifts are large. Including drifts in the theory leads to multiple resonances at the electron, ion and electric drift velocities [119, 133]. The torque, however, only changes sign at the electron drift frequency. To understand this, recall that ω represents the RMP frequency in the $E \times B$ frame. When $\omega = \omega_{*e}$ the electrons are at rest with respect to the RMP, allowing reconnection to proceed. It follows that mode penetration occurs at $\omega = \omega_{*e}$ and resonant 'braking' acts to reduce $\omega - \omega_{*e}$. Examination of figures 1 and 4 shows that although there can be a bifurcation with a discontinuous reduction of the differential rotation near the ion resonance, the rotation in the final state and the narrowness of the ion resonance are such that the screening remains strong.

The effect of diamagnetic drifts on mode penetration thresholds has been explored in experiments using the 'dynamic ergodic divertor' (DED) on the TEXTOR tokamak [132, 136–138]. In these experiments, the penetration threshold was measured for different RMP frequencies as well as for different values of the beam-power fraction $(P_{\text{co-NBI}} - P_{\text{ctr-NBI}})/(P_{\text{co-NBI}}+P_{\text{ctr-NBI}})$ describing the distribution between co- and counter-injected NBI power. The results, reproduced in figure 5, show that the penetration threshold reaches a minimum for a value of the beam input corresponding to $E \times B$ rotation in the direction of the ion diamagnetic drift (co-injection). This is consistent with theoretical expectations, since driving the plasma rotation in the co-current direction has the effect of reducing the differential velocity between the electrons and the perturbation, facilitating mode penetration. Similarly, rotating the RMP at 1 kHz in the counter direction reduces its differential velocity with respect to the electrons. As a result, for counter-rotation of the DED fields the minimum current for mode penetration occurs at much lower values of the beam fraction, as shown in figure 5.

Co-rotation of the DED fields, by contrast, increases the differential rotation such that the penetration was not observed even at the highest value of the coil current. Since the relative rotation of the DED with respect to the electrons was always in the direction of the ion drift velocity, increasing the DED current produces an electric field that acts to brake the electrons and simultaneously enhances the co-rotation of the ions. The experimental results are in agreement with numerical simulations using the drift model in cylindrical geometry [67, 139].

An interesting feature of the results is that the minimum mode-penetration current is positive in the experiment, unlike the slab theory where the threshold amplitude vanishes for $\omega = \omega_{*e}$. This finite mode-penetration threshold may reflect the stabilizing influence of favourable average curvature.

3.5. Implications for future devices

Mode penetration imposes challenging requirements on the design of the error-field control coils for future devices, including ITER. Avoidance of low-density locked modes (LDLMs) requires minimizing the amplitude of the magnetic perturbations that are resonant in the core. The tolerances for error fields become more stringent during operation near the no-wall stability limit due to the amplification of the braking force in this regime [54, 140, 141].

A recently developed technique for the mitigation of ELMs relies on the application of moderate wavelength ($n = 3$ or 4) magnetic perturbations tailored so as to maximize the amplitude of the edge-resonant harmonics. Such magnetic perturbations act to degrade the H-mode pedestal and thereby diminish or completely eliminate ELMs [142, 143]. An intriguing feature of the observations is the steepening of the electron temperature pedestal during the application of the RMP. This feature is opposite to the flattening of the profile that one expects in the presence of magnetic chaos. Another peculiarity of the ELM suppression experiments is the absence of locked-mode spin-up following the turn-off of the current in the RMP coils. Similar results were obtained in TEXTOR, where locked modes induced with the DED remained locked

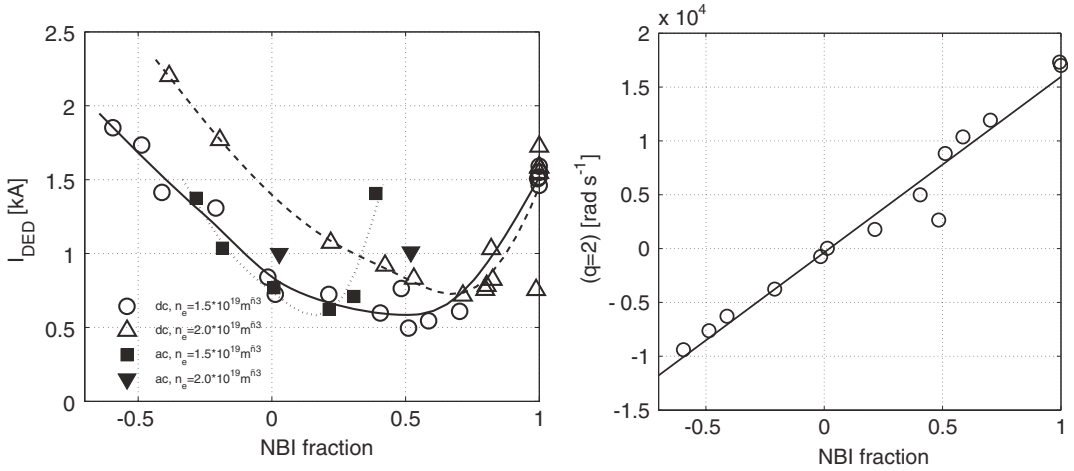

Figure 5. Penetration threshold measured in TEXTOR using the DED and a continuously tunable NBI beam-power fraction. The right-hand figure shows the rotation at the $q = 2$ surface as a function of the NBI fraction. The left-hand figure shows the critical DED current for mode penetration as a function of the power fraction. The filled symbols show data collected with the DED counter-rotating at 1 kHz and the open symbols show data for a static DED. For co-rotating DED, mode penetration was not observed up to the largest available value of I_{DED}. Reproduced with permission from [138].

until termination of the NBI [136]. In TEXTOR, however, the absence of spin-up is probably due to uncompensated residual errors. In COMPASS-D H modes, by contrast, islands were observed to spin-up reliably in $n = 1$ locked-mode experiments [144].

A possible explanation for the effects of edge-RMPs is that the very strong diamagnetic flows in the pedestal screen the perturbation, locally preserving good flux surfaces [134]. Overlapping of the electrostatic convection cells that are associated with the screening process causes convective fluxes that may substitute for magnetic chaos to produce enhanced particle transport [145, 146]. Note that a pumpout is also observed in the low mode-number ELM-mitigation experiments on JET [147, 148].

The next section describes the interaction between the profiles and a magnetic island in the case of penetrated RMP as well as for spontaneous tearing modes such as the NTM.

4. Transport in magnetic islands

The primary question regarding relaxed magnetic islands is their effect on the profiles of density, temperature, current and rotation velocity. The changes in the profiles determine the effect of the island on overall confinement, and they determine whether the island grows or decays. Our understanding of the effect of the profiles on the island amplitude informs the methods used for avoiding islands as well as for suppressing them with RF current-drive and heating.

4.1. The constant-ψ approximation

To evaluate equilibria with islands, the first obstacle is the interdependence of the profiles and the island width. Fortunately, in many cases of interest the variation of the current across the island is small compared with its background value, $J_\parallel - J_{\parallel 0}(\chi_s) \ll J_{\parallel 0}(\chi_s)$, where $J_{\parallel 0}(\chi_s)$ is the parallel component of the current in the absence of island and χ_s is the resonant surface. As a result, the variation across the layer of the resonant Fourier component of the helical flux, $\tilde{\psi}_{m,n}$, is small. The approximation that consists in neglecting this variation, known as the 'constant-$\tilde{\psi}$' approximation, greatly facilitates the analysis and interpretation of observations. It implies that just two parameters specify the magnetic geometry: the amplitude $\tilde{\psi}_{m,n}$ and phase ϕ of the resonant perturbation (for a rotating island, $\mathrm{d}\phi/\mathrm{d}t = \omega t$). In particular, the island width completely determines the shape of the island. The helical flux takes the form

$$\psi = B_0 x^2/2L_s + \tilde{\psi}_{m,n}\cos(m\theta - n\zeta - \phi), \qquad (9)$$

where x is the distance from the resonant surface, $L_s = B_0/J_{\parallel 0}(\chi_s)$ is the shear length and B_0 is the background field. Equation (9) implies that the width of the island is

$$W = 4\sqrt{\tilde{\psi}_{m,n}L_s/B_0}.$$

For intrinsic reconnecting instabilities (as opposed to RMP-driven tearing), a necessary condition for the applicability of the constant-$\tilde{\psi}$ approximation takes the form [149–151]

$$\Delta' W \ll 1. \qquad (10)$$

When the system approaches marginal ideal stability, such as for the $m = 1$ internal kink mode or for the resistive wall mode, Δ' becomes large and this condition is violated. In such cases, the constant-$\tilde{\psi}$ approximation fails and it is necessary to solve the Grad–Shafranov equation in order to determine the island geometry. The island evolution involves a competition between the rate of reconnection, which determines the growth of the island width, and the rate of current diffusion. When condition (10) is satisfied, by contrast, current diffusion is faster than reconnection and the current profile is able to relax. The relaxation of the current implies that not only $\tilde{\psi}$ but also $\partial\tilde{\psi}/\partial t$ is approximately constant across the island.

For larger islands, the flux becomes frozen-in. A critical island width appears such that the separatrix collapses into a current ribbon at the X-point, signalling the onset of Sweet–Parker reconnection [149, 151].

4.2. The generalized Rutherford equations

The constant-$\tilde{\psi}$ approximation leads to the following simple expression of the matching condition between the resonant layer and the exterior solution:

$$\Delta'_{m,n}\tilde{\psi}_{m,n} = \int \mathrm{d}x \oint \frac{\mathrm{d}\theta}{\pi} J \exp[\mathrm{i}(m\theta - n\zeta - \phi)], \qquad (11)$$

where $\Delta'_{m,n}$ is the matching parameter from the exterior solution. The helical current in equation (11) includes the perturbed inductive, bootstrap, polarization, Pfirsch–Schlüter and the beam- and RF-driven currents. A solution method is now apparent: the first step consists of solving the transport problem in the geometry specified by equation (9). The second step consists of using the result of the transport calculation to evaluate the integral in equation (11). Separating the contributions to the current from the time derivatives of $\tilde{\psi}_{m,n}$ and ϕ leads to the evolution equations for the components, respectively, in phase and in phase-quadrature with the reconnected flux,

$$\frac{\mathrm{d}W}{\mathrm{d}t} = \frac{r_\mathrm{s}^2}{\tau_\mathrm{R}}[\Delta' + \Delta(W,\omega)]; \qquad (12)$$

$$\frac{\mathrm{d}^2\phi}{\mathrm{d}t^2} = F_\mathrm{t}(W,\omega). \qquad (13)$$

The above two equations generalize the results of Rutherford [6]. The two functions $\Delta(W,\omega)$ and F_t represent, respectively, the free energy available for reconnection and the acceleration of the island caused by any imbalance of lateral forces acting on the island. The determination of these two functions is the central task of the singular-layer theory. The rest of this section describes some of the recent progress in our knowledge of the contributions to these two functions originating from the pressure-driven (Pfirsch–Schlüter and bootstrap) currents, the inductive currents and the inertia-driven (polarization) currents.

4.3. Heat transport in magnetic islands

The contributions of the Pfirsch–Schlüter [103, 111–113] and neoclassical currents [152, 153] to the island evolution have long been well understood in the limit of large islands in which the temperature profile is fully flattened. The increasing resolution in the observations of electron temperature profiles, however, have stimulated theoretical research on the characteristic width for temperature flattening. The effects of a magnetic island on the profiles of temperature are governed by the competition between parallel transport and perpendicular transport. The role of this competition in magnetic islands is analogous to that in the scrape-off layer. The controlling parameter is the connection length with respect to the magnetic axis of the island. This is the length that one must travel along a field line in order to encircle the magnetic axis of the island completely. Near the separatrix, the connection length becomes very large, reflecting the fact that the magnetic field near the X-lines is nearly parallel to the magnetic axis of the flux tube. For sufficiently long connection lengths, the parallel fluxes are no longer effective in relaxing the profiles along the field line. Equilibrium gradients may then develop within the flux surfaces.

Near the O-point of the island, the connection length $L_\mathrm{c} \sim L_\mathrm{s}/k_\theta W$ where L_s is the magnetic shear length. It follows that as the island grows, there is a characteristic width above which the parallel transport dominates and the gradients become perpendicular to the flux surfaces. In the collisional regime, the equation describing the transport near the island is [6]

$$\kappa_\parallel \nabla_\parallel^2 T + \kappa_\perp \nabla_\perp^2 T = 0.$$

The resulting critical width is [7]

$$W_\mathrm{c} \sim \left(\frac{\kappa_\parallel}{\kappa_\perp}\frac{L_\mathrm{s}}{k_\theta}\right)^{1/4}.$$

In the collisionless regime, quasilinear theory provides estimates of profile flattening for very narrow islands [154]. More recent investigations have used the drift-kinetic equation to estimate the threshold for flattening [155, 156]. Note, however, that even in the collisional regime, the competition between turbulent transport and parallel streaming is the subject of ongoing research [157].

For $W \gg W_\mathrm{c}$, the profiles inside the separatrix are flat in the absence of sources or inward pinches. Profile flattening is indeed routinely observed in experiments [158, 129], but there are also challenging observations of profile *peaking* inside large islands [159]. Profile peaking manifests itself in the observations of snakes in the core where the constant-$\tilde{\psi}$ approximation fails [126, 127], as well as for $q = 3$ islands closer to the edge. Shaing has proposed an explanation for the observations based on the improvement to the confinement resulting from plasma flow around the island [160–162].

4.4. Island saturation

An important aspect of the temperature flattening that has recently received attention is its influence on the saturation amplitude of tearing modes. As a result of the dependence of the conductivity on temperature, $\eta \sim T_\mathrm{e}^{-3/2}$, the inductive current $J_\mathrm{ind} = \eta^{-1}\partial\psi_0/\partial t$, which is generally responsible for the saturation of tearing modes, depends on whether temperature flattening has occurred [163]. A recent series of works has provided analytic expressions for the contribution of the inductive current to the Rutherford equation first using a reduced model in slab geometry [82, 83], subsequently extending the result to cylindrical geometry [164, 165], to the full MHD model (for application to RFPs) [166], and to a slab model describing NTMs [167]. The stabilizing effect of the induction current depends on second-order corrections to the magnetic flux in the island, however, and the effects of noninductive contributions to the flux have never been examined at this order. Furthermore, as pointed out by Hastie *et al* [163], for islands sufficiently large to flatten the temperature profile, global transport leads to a reduction of the core temperature $\delta T_\mathrm{e}(\chi < \chi_\mathrm{s}) \simeq W T'_{\mathrm{e}0}(\chi_\mathrm{s})$, where χ_s labels the resonant surface, that affects the external matching matrix and in particular, the Δ' parameter. The quantification of these effects is a necessary step to explain experimentally observed saturation amplitudes. In particular, the recent observations of a dependence of the saturation amplitude on the velocity shear [168, 169] may be caused by the effect of the latter on the inductive current.

4.5. Island propagation and the polarization current

Another contribution to the island evolution integrals (12)–(13) that has received recent attention is that of the polarization current. The original calculations by Smolyakov [170] and Wilson *et al* [171], contained two errors. These calculations first omitted the dominant contribution to the polarization current (thereby obtaining an incorrect sign for the result) and, second, they obtained a qualitatively incorrect value for the island rotation frequency. The two errors compensated each other when these calculations were applied to the interpretation of the observations of NTMs, thereby allowing the theory to enjoy qualitative success [120–125]. The discovery in [172] of the first of these errors, together with widespread concern over the β-limiting role of the NTM, stimulated a number of investigations of the basic properties of magnetic islands. The results of these investigations apply to rotating as well as locked islands, and to islands located in the core as well as in the edge. I summarize these results in this section.

The polarization current results from the acceleration of the plasma as it flows along the Laval nozzle formed by the flux surfaces outside the separatrix. The vector product of the acceleration and the magnetic field gives rise to a well-known ion drift with non-vanishing divergence. A parallel current must accompany this drift to maintain quasi-neutrality. This parallel current mediates the effect of the plasma flows on the island evolution [173–175].

In order to determine the distribution of the polarization current, it is necessary to know the velocity of the plasma flow with respect to the island. Since the ions and electrons experience opposite diamagnetic drifts, they cannot both be at rest with respect to the island. One finds that the velocity of the island depends on the degree of profile flattening inside the separatrix [176]. The discussion is facilitated if we express all velocities in a frame where the background electric field vanishes.

The key elements of the analysis are the frozen-in and the no-slip conditions. The frozen-in condition expresses the fact that the separatrix traps the electron fluid whenever the island is sufficiently wide. This condition applies when the skin time for magnetic diffusion across the island exceeds the time taken by the electron fluid to drift across the island due to diamagnetic effects. The expression of this condition in terms of the island width is $W > \rho_s\sqrt{C}$, where $C = (L_s/L_n)^2(\nu_e/\omega_{*e})(m_e/m_i) < 1$ is a measure of the collisionality (the bound $C < 1$ corresponds to the semi-collisional regime that describes most fusion experiments) [177]. Note that the frozen-in condition is generally violated in suppressed island, allowing the plasma to stream through the island. The second condition, the no-slip condition, expresses the fact that the much greater viscosity of the ion fluid compared with the electron fluid results in the continuity of the ion velocity across the separatrix. This second condition is satisfied in suppressed as well as in relaxed islands.

The frozen-in and no-slip conditions lead to the following expression for the island velocity u:

$$u = v_{De}^{\mathrm{in}} + v_{Di}^{\mathrm{out}} - v_{Di}^{\mathrm{in}}, \tag{14}$$

where the v_{Ds} are the diamagnetic drifts, the index $s = \mathrm{i}, \mathrm{e}$ labels the species and the superscripts indicate on which side of the separatrix the quantity is measured. The jump condition expressed by equation (14) is illustrated in figure 6. To avoid unnecessarily burdening the notation, we will assume that the island is sufficiently wide that the electron temperature is fully flattened inside the separatrix. We further assume that the degree of flattening of the ion temperature is equal to that of the density. The diamagnetic velocities are then

$$v_{Ds}^{\mathrm{in}} = f v_{Ds}^{\mathrm{out}},$$

where f is a flattening factor varying between 0 and 1 that describes the ratio of the density gradient at the O-point of the island to the density gradient in the reference state. Substituting the diamagnetic drifts into the equation for the island velocity yields

$$u = f v_{*e}^{\mathrm{out}} + (1 - f) v_{*i}^{\mathrm{out}},$$

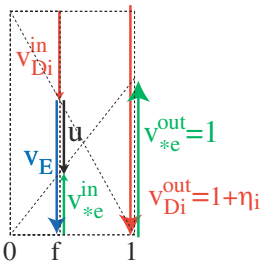

Figure 6. Graphical solution for the island propagation velocity in terms of the profile flattening factor f.

The preceding analysis shows that islands that are sufficiently thin for the density and ion temperature gradient to be maintained ($f = 1$) propagate at the electron diamagnetic drift velocity. Note that electrons outside the separatrix, however, are propagating at $1+\eta_e$ times the diamagnetic velocity, where η_s is the ratio of the background density scale-length and the temperature scale-length of species s. In the opposite limit of large islands in which the ion pressure is fully flattened ($f = 0$), the island propagates at the ion pressure drift velocity, or $-(1 + \eta_i)\tau\omega_{*e}$ where $\tau = T_i/T_e$ is the temperature ratio. That is, the ions outside the separatrix are at rest with respect to the island.

The above discussion leaves unanswered the question of the characteristic width for density flattening, W_{flatg}. This question is controversial and estimates have differed by more than an order of magnitude, from the semi-collisional boundary $W_{\mathrm{flatg}} \sim \rho_s\sqrt{C}$ [117] to the drift-acoustic width $W_{\mathrm{flatg}} \sim \rho_s L_s/L_n$ at which the drift-wave couples with ion-acoustic waves [62, 64, 115]. Numerical results for $C < 1$, however, suggest that the coupling of the island to drift waves can flatten the profiles even in the absence of ion-acoustic waves, for $k_\parallel c_s \ll \omega_*$. An estimate consistent with the available theoretical results is $W_{\mathrm{flatg}} \sim \rho_s \max(1, C^{1/2})$. This estimate is qualitatively consistent with observations in LHD (figure 9) showing that the electric field inside the $m = n = 1$ island drops to zero for $W \gtrsim 1$ cm [128, 130]. It is also qualitatively consistent with other observations in the same experiment showing a clear increase in the iso-density width with collision frequency and a decrease with β [129].

Experiments that use RMPs to successively lock and release magnetic islands provide another source of data on

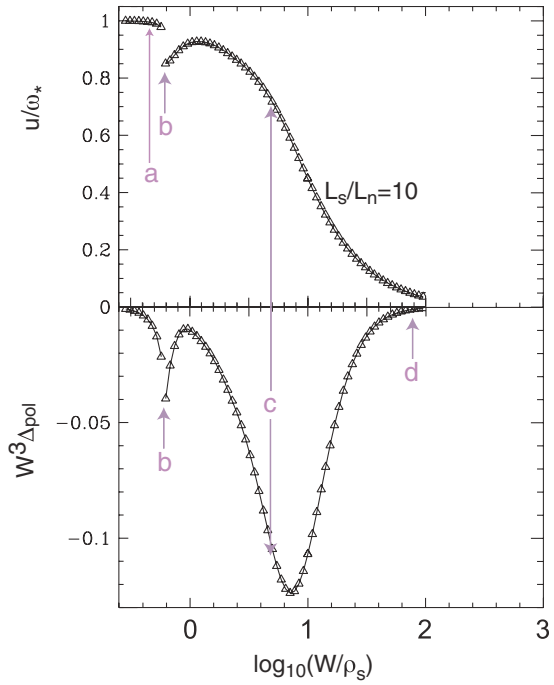

Figure 7. Dependence of the island propagation velocity u and of the contribution of the polarization current to the Rutherford equation, $\Delta_{\rm pol}$, on the island width. Note that $\Delta_{\rm pol}$ is scaled to the cube of the island width. The labelled points along the curve refer to the values of W for which the velocity profiles are shown in figure 8.

profile flattening. During the locked phase, the island grows as the result of the additional drive provided by the RMP. Since the reconnection time is much slower than the momentum confinement time, removal of the RMP causes the island to spin up to its natural velocity while temporarily retaining the larger size it acquired during the locked phase. Observations in COMPASS-C show that the rotation frequency of the island after the locked phase is reduced by 20% of the diamagnetic frequency, providing evidence of the increased density flattening associated with the larger size of the island [77].

Lastly, measurements of the rotation velocity of NTMs in DIII-D have found that the islands were rotating in the ion direction, consistent with ion pressure flattening [178]. These data are also consistent with the observations of a threshold for the excitation of the NTM, given the stabilizing effect of the polarization current for islands rotating in the ion direction.

Since islands of width $W \gtrsim W_{\rm flatg}$ are approximately co-rotating with the ions, it is natural to expect the polarization drift to become small for these islands. Surprisingly, numerical simulations in the collisional regime, $C \gg 1$, show that this is not the case [118]. Figure 7 shows the results of simulations of the unforced propagation of an island. The simulations are for a plasma with cold ions. The figure shows the dependence of the propagation velocity u and of the parameter $\Delta_{\rm pol}$ representing the contribution of the polarization current to the Rutherford equation for the evolution of the island width. Note that in figure 7, $\Delta_{\rm pol}$ is scaled with the cube of the island width to facilitate comparison with analytic estimates that predict $\Delta_{\rm pol} = a_{\rm pol}\, u^2/W^3$, where $a_{\rm pol}$ is a coefficient that depends on the profile of the ion velocity across the island. The numerically obtained $a_{\rm pol}$ exhibits a pronounced resonance when the island width is such that the drift-wave couples strongly to ion-acoustic waves. The corresponding resonance condition is $\omega_* = k_\parallel c_{\rm s}$, or $W = \rho_{\rm s} L_{\rm s}/L_{\rm n}$. Analysis of the diffusion of momentum in an island with fully flattened profile shows that the resonance manifests itself as a singularity of the Reynolds stress appearing in the diffusion equation [179]. This resonance is robustly stabilizing and may determine the effective threshold for the onset of NTMs.

Figure 8 shows a series of profiles for various characteristic island widths marked in figure 7. The upper plots in figure 8 show the profiles of the velocity of ions (solid curves) and electrons (dashed curves) in a section of the island traversing the O-point, while the lower plots show the profiles of the density across both the X-point (solid curves) and O-point (dashed curves). The width of the island is indicated by the vertical grey band. At the O-point ($x = 0$), the island velocity (horizontal dashed line) always matches the electron velocity. This is a manifestation of the frozen-in condition. It follows that the island velocity matches the diamagnetic frequency at the O-point, the latter being reduced by the flattening of the density evident in the profiles shown in the bottom figures. The ion velocity is identical to the electric drift velocity in these cold-ion simulations. Its value remains much smaller than the electron drift velocity at all widths. Note that for small widths the ion velocity is very different from that of the island, indicating a rapid streaming of the ions through the separatrix. As the island exceeds the ion-sound Larmor radius, there is a tendency for the ions to be entrained by the island: this is noticeable in figure 8(c) showing the case $\rho_{\rm s}/W = 0.1$.

It is interesting to compare the profiles of figure 8 with the profiles of the electric field measured in the $m/n = 1/1$ island in the edge of the LHD stellarator shown in figure 9. The width of this island is controlled by external coils and can be varied between 0% and 20% of the minor radius. As a result of the finite ion temperature in LHD, the profile flattening inside the island gives rise to a jump in the ion drift velocity across the separatrix. To satisfy the no-slip condition, this jump is compensated by a discontinuity in the electric field. Note that mode penetration has already occurred at the lowest nonzero value of the current in figure 9. The 1/1 island in LHD is technically a locked mode, but the velocity shear outside the island is small so that the viscous forces acting on the island are unlikely to play an important role.

4.6. Interaction of turbulence and magnetic islands

Recent investigations have examined the interaction between turbulence and magnetic islands. Itoh *et al* have investigated the conditions under which turbulent fluctuations can overcome the stability threshold for the NTM [180, 181]. Their theory offers an explanation for the frequent occurrence of NTMs in the absence of a macroscopic triggering event. McDevitt and Diamond have calculated the evolution of the drift-wave population density in the presence of a tearing mode using the wave-kinetic equation to model the turbulence. They concluded that the turbulence gives rise to a negative viscosity that acts as a pump on the resonant long-wavelength mode [182]. The negative viscosity combined with the

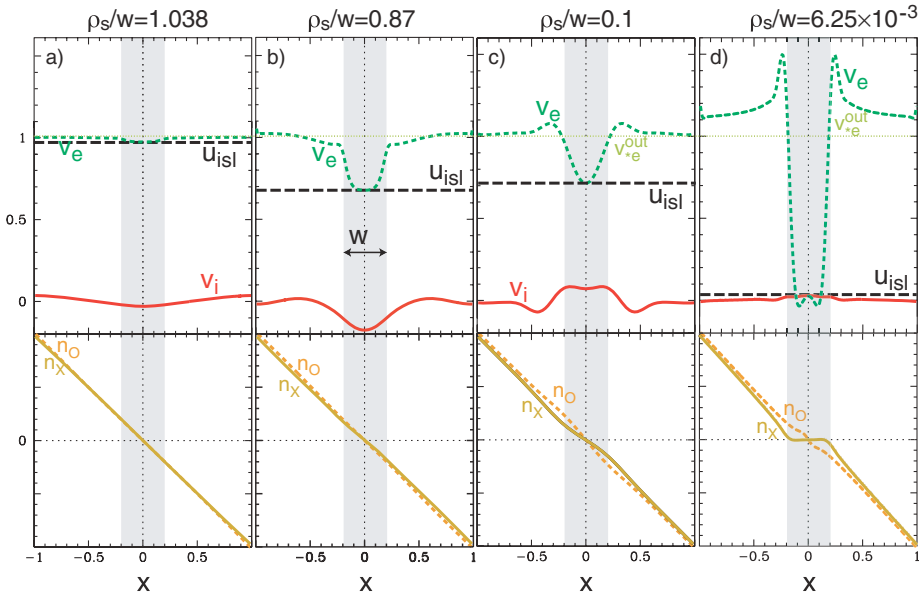

Figure 8. Profiles of the electron and ion velocities across the O-point of an island for the three widths marked in figure 7.

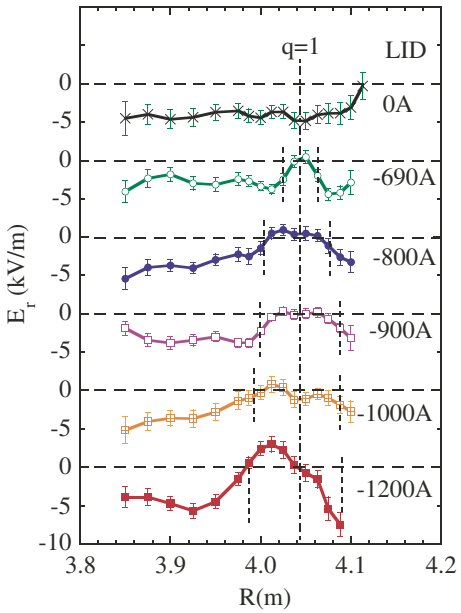

Figure 9. Profiles of the electron and ion velocities across the O-point of the $m/m = 1/1$ island in the LHD stellarator for various island widths obtained by increasing the current in the external coil. Reproduced from [130] with permission.

coupling of the tearing mode to zonal flows results in asymptotic oscillations of the wavefunction.

Ishizawa *et al* have carried out numerical simulations of the evolution of the double-tearing mode in the presence of electromagnetic turbulence. They found that in a first stage, the zonal flows driven by the turbulence stabilize the linearly unstable double-tearing mode. In a second stage, however, long-wavelength magnetic fluctuations exert a drag that suppresses the zonal flows, leading to the rapid growth of the double-tearing mode [68]. Lastly, Militello *et al* have shown that turbulence reduces the propagation velocity of the island [183]. Its effect is destabilizing for thin islands but becomes stabilizing, primarily due to the reduced propagation velocity, for islands greater than a few times the Larmor radius. Note that simulations of the interaction of turbulence with magnetic islands generally use transport coefficients of magnitude comparable to the anomalous transport coefficients in experiments. The appropriateness of using such macroscopic transport coefficients for narrow structures like magnetic islands is a subject of current research [184]. The investigation of this subject requires the use of 3D simulations [68, 185], since in 2D the flattening of the gradients by the island tends to stabilize the microinstabilities driving the turbulence [183].

5. Discussion

Magnetic islands play an important role in all magnetic confinement devices including RFPs, stellarators and tokamaks. Avoidance of tearing modes by control of the discharge conditions and control of the islands themselves has progressed to the extent that they no longer present a substantial threat to the confinement of fusion plasmas away from the ideal stability limits. As a result, the focus of research has shifted to using islands as the agents of plasma control systems. Examples include the use of islands for driving current in the core, [46] for mitigating ELMs [142] and for controlling transport in the edge of stellarators [158].

The extraordinary resolution provided by modern diagnostic systems provides unprecedented opportunities for testing and improving our knowledge of the physics of magnetic islands. In particular, the detailed measurements of the profiles of temperature, density and velocity inside a variety of islands is challenging theory and breaking down conventional barriers between the study of macroscopic and microscopic plasma dynamics. For example, improved understanding of the interaction between magnetic islands and turbulence may make it possible to use long-wavelength magnetic fluctuation data to acquire information on turbulent dynamics.

Theory has played an important role in developing our present abilities with regard to magnetic islands. In addition to predicting pressure-driven healing in stellarators [103] and the growth of NTMs in tokamaks [152], theoretical understanding has guided the development of techniques for using RF current drive to suppress islands [186]. Although analytic results and simulations have proven to be useful guides for interpreting experiments and providing qualitative predictions, many challenges must be overcome before we can achieve quantitative prediction capabilities. The renewed interest in the development of computational tools for predicting the effects of external coils on 3D waveforms [95] is encouraging in view of the limitations affecting initial-value codes. In the near term, however, the progress demonstrated by initial-value codes with regard to the performance of two-fluid time steppers [58, 69] and anisotropic heat transport [187, 188] is likely to place them at the forefront of advances in our understanding of island physics.

Acknowledgments

Research funded by the US Department of Energy under contracts # DE-FG03-96ER-54346 and DE-FC02-04ER54785.

References

[1] Spitzer L. 1958 *Phys. Fluids* **1** 253
[2] Hazeltine R.D. and Meiss J.D. 1985 *Phys. Rep.* **121** 1
[3] Mirnov S.V. and Semenov I.B. 1971 *At. Energy.* **30** 14
[4] Hosea J.C., Jobes F.C., Hickok R.L. and Dellis A.N. 1973 *Phys. Rev. Lett.* **30** 839
[5] Matsuda S. and Yoshikawa M. 1975 *Japan. J. Appl. Phys.* **14** 87
[6] Rutherford P.H. 1973 *Phys. Fluids* **16** 1903
[7] Fitzpatrick R. 1995 *Phys. Plasmas* **2** 825
[8] Spakman G.W. *et al* and the TEXTOR Team 2008 *Nucl. Fusion* **48** 115005 (10pp)
[9] Chang Z. *et al* 1994 *Nucl. Fusion* **34** 1309
[10] Yu Q. 2006 *Phys. Plasmas* **13** 062310
[11] Tokar M.Z. and Gupta A. 2007 *Phys. Rev. Lett.* **99** 225001
[12] Holzl M., Günter S. and ASDEX Upgrade Team 2008 *Phys. Plasmas* **15** 072514
[13] Strumberger E., Günter S., Schwarz E. and Tichmann C. 2008 *New J. Phys.* **10** 023017
[14] McCormick K. *et al* 2003 *J. Nucl. Mater.* **313–316** 1131
[15] Grigull P. *et al* 2003 *J. Nucl. Mater.* **313–316** 1287
[16] Morisaki T. *et al* 2005 *J. Nucl. Mater.* **337–339** 154
[17] Reiman A., Zarnstorff M., Monticello D., Weller A., Geiger J. and the W7-AS Team 2007 *Nucl. Fusion* **47** 572
[18] Rosenbluth M.N., Sagdeev R.Z., Taylor J.B. and Zaslavsky G.M. 1966 *Nucl. Fusion* **6** 297
[19] Rechester A.B. and Rosenbluth M.N. 1978 *Phys. Rev. Lett.* **40** 38
[20] Lichtenberg A., Itoh K., Itoh S.-I. and Fukuyama A. 1992 *Nucl. Fusion* **32** 495
[21] Breslau J.A., Jardin S.C. and Park W. 2007 *Phys. Plasmas* **14** 056105
[22] Igochine V., Dumbrajs O., Zohm H. and the ASDEX Upgrade Team 2008 *Nucl. Fusion* **48** 062001
[23] Cappello S. and Biskamp D. 1996 *Nucl. Fusion* **36** 571
[24] Ho Y.L. and Craddock G.G. 1991 *Phys. Fluids* B **3** 721
[25] Sovinec C.R., Gianakon T.A., Held E.D., Kruger S.E., Schnack D.D. and N. Team 2003 *Phys. Plasmas* **10** 1727
[26] Sarff J.S., Hokin S.A., Ji H., Prager S.C. and Sovinec C.R. 1994 *Phys. Rev. Lett.* **72** 3670
[27] Martin P. *et al* 2003 *Nucl. Fusion* **43** 1855
[28] Frassinetti L., Alfier A., Pasqualotto R., Bonomo F. and Innocente P. 2008 *Nucl. Fusion* **48** 045007
[29] Wong K.L., Kaye S., Mikkelsen D.R., Krommes J.A., Hill K., Bell R. and LeBlanc B. 2008 *Phys. Plasmas* **15** 056108
[30] Tokar M., Evans T., Gupta A., Kalupin D., Nicolai A., Singh R. and Unterberg B. 2008 *Nucl. Fusion* **48** 024006
[31] Evans T.E. *et al* 2006 *Phys. Plasmas* **13** 056121
[32] Joseph I. *et al* 2008 *Nucl. Fusion* **48** 045009
[33] Zohm H. 1997 *Phys. Plasmas* **4** 3433
[34] Gantenbein G., Zohm H., Giruzzi G., Günter S., Leuterer F., Maraschek M., Meskat J., Yu Q., ASDEX Upgrade Team and ECRH-Group (AUG) 2000 *Phys. Rev. Lett.* **85** 1242
[35] Petty C.C., La Haye R.J., Luce T.C., Humphreys D.A., Hyatt A.W., Lohr J., Prater R., Strait E.J. and Wade M.R. 2004 *Nucl. Fusion* **44** 243
[36] Isayama A., Oyama N., Urano H., Suzuki T., Takechi M., Hayashi N., Nagasaki K., Kamada Y., Ide S., Ozeki T. and the JT-60 team 2007 *Nucl. Fusion* **47** 773
[37] Yu Q., Zhang X.D. and Günter S. 2004 *Phys. Plasmas* **11** 1960
[38] Humphreys D.A., Ferron J.R., La Haye R J, Luce T.C., Petty C.C., Prater R. and Welander A.S. 2006 *Phys. Plasmas* **13** 056113
[39] Westerhof E. *et al* 2007 *Nucl. Fusion* **47** 85
[40] Brennan D.P. *et al* 2003 *Phys. Plasmas* **10** 1643
[41] Brennan D.P., Strait E.J., Turnbull A.D., Chu M.S., La Haye R.J., Luce T.C., Taylor T.S., Kruger S. and Pletzer A. 2002 *Phys. Plasmas* **9** 2998
[42] Pustovitov V. 2005 *Nucl. Fusion* **45** 245
[43] La Haye R.J., Politzer P.A. and Brennan D.P. 2008 *Nucl. Fusion* **48** 015005
[44] Luce T. *et al* 2003 *Nucl. Fusion* **43** 321
[45] Wade M.R. *et al* 2005 *Nucl. Fusion* **45** 407
[46] Chu M.S., Chan V.S., Politzer P.A., Brennan D.P., Choi M., Lao L.L., John H.E.S. and Turnbull A.D. 2006 *Phys. Plasmas* **13** 114501
[47] Lazzaro E. *et al* and M.S.C. to the EFDA-JET work programme 2002 *Phys. Plasmas* **9** 3906
[48] La Haye R.J., Rettig C.L., Groebner R.J., Hyatt A.W. and Scoville J.T. 1994 *Phys. Plasmas* **1** 373
[49] La Haye R.J., Groebner R.J., Hyatt A.W. and Scoville J.T. 1993 *Nucl. Fusion* **33** 349
[50] Solomon W.M., Kaye S.M., Bell R.E., LeBlanc B.P., Menard J.E., Rewoldt G., Wang W., Levinton F.M., Yuh H. and Sabbagh S.A. 2008 *Phys. Rev. Lett.* **101** 065004
[51] Ebrahimi F., Mirnov V.V. and Prager S.C. 2008 *Phys. Plasmas* **15** 055701
[52] Lazarus E.A. *et al* 2006 *Plasma Phys. Control. Fusion* **48** L65
[53] Morris A.W., Carolan P.G., Fitzpatrick R., Hender T.C. and Todd T.N. 1992 *Phys. Fluids* B **4** 413
[54] La Haye R.J., Hyatt A.W. and Scoville J.T. 1992 *Nucl. Fusion* **32** 2119
[55] La Haye R.J., Fitzpatrick R., Hender T.C., Morris A.W., Scoville J.T. and Todd T.N. 1992 *Phys. Fluids* B **4** 2098
[56] Aydemir A.Y., Wiley J.C. and Ross D.W. 1989 *Phys. Fluids* B **1** 774
[57] Lütjens H., Luciani J.-F. and Garbet X. 2001 *Phys. Plasmas* **8** 4267
[58] Strauss H., Sugiyama L., Fu G., Park W. and Breslau J. 2004 *Nucl. Fusion* **44** 1008
[59] Maget P., Huysmans G.T.A., Garbet X., Ottaviani M., Lütjens H. and Luciani J.-F. 2007 *Phys. Plasmas* **14** 052509
[60] Lütjens H. and Luciani J.-F. 2008 *J. Computat. Phys.* **227** 6944
[61] Biskamp D. 1979 *Nucl. Fusion* **19** 777
[62] Biskamp D. 1978 *Nucl. Fusion* **18** 1059
[63] Monticello D.A. and White R.B. 1980 *Phys. Fluids* **23** 366
[64] Hicks H.R., Carreras B.A. and Holmes J.A. 1984 *Phys. Fluids* **27** 909

[65] Finn J.M. 1998 *Phys. Plasmas* **5** 3595
[66] Yu Q., Günter S. and Scott B.D. 2003 *Phys. Plasmas* **10** 797
[67] Yu Q., Günter S., Kikuchi Y. and Finken K. 2008 *Nucl. Fusion* **48** 024007
[68] Ishizawa A. and Nakajima N. 2007 *Phys. Plasmas* **14** 040702
[69] Murphy N.A. and Sovinec C.R. 2008 *Phys. Plasmas* **15** 042313
[70] Yu Q. and Günter S. 1998 *Plasma Phy. Control. Fusion* **40** 1989
[71] Yu Q., Günter S., Lackner K., Gude A. and Maraschek M. 2000 *Nucl. Fusion* **40** 2031
[72] Sugiyama L.E. and Park W. 2000 *Phys. Plasmas* **7** 4644
[73] Chandra D., Sen A., Kaw P., Bora M. and Kruger S. 2005 *Nucl. Fusion* **45** 524
[74] Yu Q. and Günter S. 2008 *Nucl. Fusion* **48** 065004
[75] Hazeltine R.D. and Meiss J.D. 2003 *Plasma Confinement* (New York: Dover)
[76] Fitzpatrick R. 1993 *Nucl. Fusion* **33** 1049
[77] Hender T.C. *et al* 1992 *Nucl. Fusion* **32** 2091
[78] Reiman A.H. and Monticello D.A. 1992 *Nucl. Fusion* **32** 1341
[79] Fishpool G.M. and Haynes P.S. 1994 *Nucl. Fusion* **34** 109
[80] Buttery R.J. *et al* and J. Team, C.-D.R. Team and D.-D. Team 1999 *Nucl. Fusion* **39** 1827
[81] Pletzer A., Bondeson A. and Dewar R.L. 1994 *J. Comput. Phys.* **115** 530
[82] Escande D.F. and Ottaviani M. 2004 *Phys. Lett.* A **323** 278
[83] Militello F. and Porcelli F. 2004 *Phys. Plasmas* **11** L13
[84] Furth H.P., Rutherford P.H. and Selberg H. 1973 *Phys. Fluids* **16** 1054
[85] Boozer A.H. 1999 *Phys. Plasmas* **6** 831
[86] Nuhrenberg C. and Boozer A.H. 2003 *Phys. Plasmas* **10** 2840
[87] Chu M. *et al* 2007 *Nucl. Fusion* **47** 434
[88] Tokar M.Z., Evans T.E., Singh R. and Unterberg B. 2008 *Phys. Plasmas* **15** 072515
[89] Cole A.J., Hegna C.C. and Callen J.D. 2008 *Phys. Plasmas* **15** 056102
[90] Zhu W. *et al* 2006 *Phys. Rev. Lett.* **96** 225002
[91] Grimm R.C., Dewar R.L., Manickam J., Jardin S.C., Glasser A.H. and Chance S.M. 1983 Resistive instabilities in tokamak geometry *Plasma Physics and Controlled Nuclear Fusion Research 1982* vol 3 (Vienna: IAEA) pp 35–47
[92] Waelbroeck F.L. 1999 *Phys. Plasmas* **6** 1208
[93] Chu M.S., La Haye R.J., Austin M.E., Lao L.L., Lazarus E.A., Pletzer A., Ren C., Strait E.J., Taylor T.S. and Waelbroeck F.L. 2002 *Phys. Plasmas* **9** 4584
[94] Connor J.W., Cowley S.C., Hastie R.J., Hender T.C., Hood A. and Martin T.J. 1988 *Phys. Fluids* **31** 577
[95] Park J.-K., Boozer A.H. and Glasser A.H. 2007 *Phys. Plasmas* **14** 052110
[96] Park J.-K., Boozer A.H., Menard J.E. and Schaffer M.J. 2008 *Nucl. Fusion* **48** 045006
[97] Fitzpatrick R., Hastie R., Martin T. and Roach C. 1993 *Nucl. Fusion* **33** 1533
[98] Fitzpatrick R. and Hender T.C. 1994 *Phys. Plasmas* **1** 3337
[99] Hirshman S.P. and Betancourt O. 1991 *J. Comput. Phys.* **96** 99
[100] Nakamura Y., Suzuki Y., Yamagishi O., Kondo K., Nakajima N., Hayashi T., Monticello D. and Reiman A. 2004 *Nucl. Fusion* **44** 387
[101] Reiman A. and Greenside H. 1986 *Comput. Phys. Commun.* **43** 157
[102] Narihara K. *et al* 2001 *Phys. Rev. Lett.* **87** 135002
[103] Cary J.R. and Kotschenreuther M. 1985 *Phys. Fluids* **28** 1392
[104] Hegna C.C. and Bhattacharjee A. 1989 *Phys. Fluids* B **1** 392
[105] Bhattacharjee A., Hayashi T., Hegna C.C., Nakajima N. and Sato T. 1995 *Phys. Plasmas* **2** 883
[106] Drake J.F. and Antonsen T.M. 1984 *Phys. Fluids* **27** 898
[107] Connor J.W. and Wilson H.R. 1995 *Phys. Plasmas* **2** 4575
[108] Sydora R.D. 2001 *Phys. Plasmas* **8** 1929
[109] Wan W. Chen Y. and Parker S.E. 2005 *Phys. Plasmas* **12** 012311
[110] Waelbroeck F.L. 1989 *Phys. Fluids* B **1** 2372
[111] Kotschenreuther M., Hazeltine R.D. and Morrison P.J. 1985 *Phys. Fluids* **28** 294
[112] Hegna C.C. and Callen J.D. 1994 *Phys. Plasmas* **1** 2308
[113] Hegna C.C. 1999 *Phys. Plasmas* **6** 3980
[114] Scott B.D. and Hassam A.B. 1987 *Phys. Fluids* **30** 90
[115] Scott B.D., Hassam A.B. and Drake J.F. 1985 *Phys. Fluids* **28** 275
[116] Parker R.D. 1993 *Proc. 19th EPS-ICPP Conf. (Innsbruck, Austria, 1992)* vol 1, ed K. Bethge (Geneva: European Physical Society) p 427
[117] Ottaviani M., Porcelli F. and Grasso D. 2004 *Phys. Rev. Lett.* **93** 075001
[118] Fitzpatrick R., Waelbroeck F.L. and Militello F. 2006 *Phys. Plasmas* **13** 122507
[119] Fitzpatrick R. and Hender T.C. 1991 *Phys. Fluids* B **3** 644
[120] Sauter O *et al* 1997 *Phys. Plasmas* **4** 1654
[121] La Haye R.J. and Sauter O. 1998 *Nucl. Fusion* **38** 987
[122] Günter S., Gude A., Maraschek M., Yu Q. and the ASDEX Upgrade Team 1999 *Plasma Phys. Control. Fusion* **41** 767
[123] Sauter O. *et al* 2002 *Plasma Phys. Control. Fusion* **44** 1999
[124] Buttery R.J., Hender T.C., Howell D.F., La Haye R.J., Sauter O., Testa D. and contributors to the EFDA-JET Work programme 2003 *Nucl. Fusion* **43** 69
[125] La Haye R. 2006 *Phys. Plasmas* **13** 055501
[126] Wesson J.A. 1995 *Plasma Phys. Control. Fusion* **37** A337
[127] Giovannozzi E., Annibaldi S., Buratti P., Frigione D., Lazzaro E., Panaccione L. and Tudisco O. 2004 *Nucl. Fusion* **44** 226
[128] Ida K. *et al* 2002 *Phys. Rev. Lett.* **88** 015002
[129] Tanaka K. *et al* 2002 *Plasma Phys. Control. Fusion* **44** A231
[130] Ida K. *et al* 2004 *Plasma Phys. Control. Fusion* **44** 290
[131] Boozer A.H. 1996 *Phys. Plasmas* **3** 4620
[132] De Bock M., Classen I.G.J., Busch C., Jaspers R.J.E., Koslowski H.R., Unterberg B. and the TEXTOR Team 2008 *Nucl. Fusion* **48** 015007
[133] Waelbroeck F.L. 2003 *Phys. Plasmas* **10** 4040
[134] Heyn M.F., Ivanov I.B., Kasilov S.V., Kernbichler W., Joseph I., Moyer R.A. and Runov A.M. 2008 *Nucl. Fusion* **48** 024005
[135] Boozer A.H. 2001 *Phys. Rev. Lett.* **86** 5059
[136] Finken K.H. *et al* 2005 *Phys. Rev. Lett.* **94** 015003
[137] Koslowski H., Liang Y., Krämer-Flecken A., Löwenbrück K., von Hellermann M., Westerhof E., Wolf R.C., Zimmermann O. and the TEXTOR team 2006 *Nucl. Fusion* **46** L1
[138] Koslowski H.R. *et al* 2006 *Plasma Phys. Control. Fusion* **48** B53
[139] Kikuchi Y., de Bock M.F.M. and Finken K.H. 2006 *Phys. Rev. Lett.* **97** 085003
[140] Garofalo A.M. *et al* 1999 *Phys. Rev. Lett.* **82** 3811
[141] Garofalo A.M., La Haye R.J. and Scoville J.T. 2002 *Nucl. Fusion* **42** 1335
[142] Evans T.E. *et al* 2003 *Phys. Rev. Lett.* **92** 235003
[143] Fenstermacher M.E. *et al* 2008 *Phys. Plasmas* **15** 056122
[144] Colton A.L., Buttery R.J., Fielding S.J., Hender T.C., Leahy P. and Morris A.W. 1999 *Nucl. Fusion* **39** 551
[145] Nardon E., Bécoulet M., Huysmans G. and Czarny O. 2007 *Phys. Plasmas* **14** 092501
[146] Izzo V. and Joseph I. 2008 *Nucl. Fusion* **48** 115004
[147] Liang Y. *et al* 2007 *Phys. Rev. Lett.* **98** 265004
[148] Liang Y. *et al* and J.-E. Contributors 2007 *Plasma Phys. Control. Fusion* **49** B581
[149] Waelbroeck F.L. 1993 *Phys. Rev. Lett.* **70** 3259
[150] Waelbroeck F.L. 1994 *J. Plasma Phys.* **50** 477
[151] Loureiro N.F., Cowley S.C., Dorland W.D., Haines M.G. and Schekochihin A.A. 2005 *Phys. Rev. Lett.* **95** 235003
[152] Carrera R., Hazeltine R.D. and Kotschenreuther M.T. 1986 *Phys. Fluids* **29** 899

[153] Hegna C.C. 1998 *Phys. Plasmas* **5** 1767
[154] Hazeltine R.D. and Strauss H. 1976 *Phys. Rev. Lett.* **37** 102
[155] Gorelenkov N.N., Budny R.V., Chang Z., Gorelenkova M.V. and Zakharov L.E. 1996 *Phys. Plasmas* **3** 3379
[156] Hazeltine R.D., Helander P. and Catto P.J. 1997 *Phys. Plasmas* **4** 2920
[157] Lecomte M., Beyer P., Garbet X. and Benkadda S. 2009 *Phys. Rev. Lett.* **102** 045006
[158] Inagaki S. *et al* 2004 *Phys. Rev. Lett.* **92** 055002
[159] de Vries P.C. *et al* 1997 *Nucl. Fusion* **37** 1641
[160] Shaing K.C. 2001 *Phys. Rev. Lett.* **87** 245003
[161] Shaing K., Hegna C., Callen J. and Houlberg W. 2003 *Nucl. Fusion* **43** 258
[162] Shaing K.C. 2003 *Phys. Plasmas* **10** 4728
[163] Hastie R.J., Militello F. and Porcelli F. 2005 *Phys. Rev. Lett.* **95** 065001
[164] Arcis N., Escande D.F. and Ottaviani M. 2006 *Phys. Plasmas* **13** 052305
[165] Militello F., Hastie R.J. and Porcelli F. 2006 *Phys. Plasmas* **13** 112512
[166] Arcis N., Escande D.F. and Ottaviani M. 2007 *Phys. Plasmas* **14** 032308
[167] Militello F. Ottaviani M. and Porcelli F. 2008 *Phys. Plasmas* **15** 042104
[168] La Haye R.J. and Buttery R.J. 2009 *Phys. Plasmas* **16** 022107
[169] Buttery R.J., La Haye R.J., Gohil P., Jackson G.L., Reimerdes H., Strait E.J. and the DIII-D Team 2008 *Phys. Plasmas* **15** 056115
[170] Smolyakov A.I. 1993 *Plasma Phys. Control. Fusion* **35** 657
[171] Wilson H.R. *et al* 1996 *Phys. Plasmas* **3** 248
[172] Waelbroeck F.L. and Fitzpatrick R. 1997 *Phys. Rev. Lett.* **78** 1703
[173] Connor J.W., Waelbroeck F.L. and Wilson H.R. 2001 *Phys. Plasmas* **8** 2835
[174] Waelbroeck F.L., Connor J.W. and Wilson H.R. 2001 *Phys. Rev. Lett.* **87** 215003
[175] James M. and Wilson H.R. 2006 *Plasma Phys. Control. Fusion* **48** 1647
[176] Waelbroeck F.L. 2005 *Phys. Rev. Lett.* **95** 035002
[177] Drake J.F., Antonsen J.T.M., Hassam A.B. and Gladd N.T. 1983 *Phys. Fluids* **26** 2509
[178] La Haye R.J., Petty C.C., Strait E.J., Waelbroeck F.L. and Wilson H.R. 2003 *Phys. Plasmas* **10** 3644
[179] Fitzpatrick R., Watson P. and Waelbroeck F.L. 2005 *Phys. Plasmas* **12** 082510
[180] Itoh S.-I., Itoh K. and Yagi M. 2003 *Phys. Rev. Lett.* **91** 045003
[181] Itoh S.-I., Itoh K. and Yagi M. 2004 *Plasma Phys. Control. Fusion* **46** 123
[182] McDevitt C.J. and Diamond P. 2006 *Phys. Plasmas* **13** 032302
[183] Militello F., Waelbroeck F.L., Fitzpatrick R. and Horton W. 2008 *Phys. Plasmas* **15** 050701
[184] Ishizawa A. and Nakajima N. 2008 *Phys. Plasmas* **15** 084504
[185] Ishizawa A. and Nakajima N. 2007 *Nucl. Fusion* **47** 1540
[186] Hegna C.C. and Callen J.D. 1997 *Phys. Plasmas* **4** 2940
[187] Sovinec C.R. *et al* 2004 *J. Comput. Phys.* **195** 355
[188] Günter S., Yu. Q., Krueger J. and Lackner K. 2005 *J. Comput. Phys.* **209** 354